JOURNAL OF CATALYSIS 112, 453–463 (1988)

Spectroscopic and Catalytic Study of P-Modified ZSM-5

A. RAHMAN, G. LEMAY, A. ADNOT, AND S. KALIAGUINE[1]

Department of Chemical Engineering, GRAPS and CRAM, Université Laval, Ste-Foy, Québec, Canada G1K 7P4

Received September 22, 1987; revised February 24, 1988

Postsynthesis modification of ZSM-5 with phosphorus was performed by gas-phase adsorption of triphenylphosphine. IR spectra of adsorbed pyridine indicated an interaction of phosphorus species with Brønsted acid sites. ESCA analysis of noncalcined catalysts suggests a model for this interaction. A quantitative treatment of ESCA intensity ratios for the calcined catalysis before and after grinding allows one to calculate the size and loading of both extraparticle and intra-pore-lattice (IPL) phosphorus oxide particles. The IPL loading was found to be very close to the loading of exchanged phosphorus calculated from the IR of adsorbed pyridine. The product distribution of MTG conversion was found to be correlated with the extent of Brønsted acid site poisoning following exchange with phosphorus species.

INTRODUCTION

Over the past few years (*1–7*) postsynthesis modifications of ZSM-5 have been proposed either as methanol-to-olefin (MTO) catalysts or in attempts to design paraselective catalysts. Kaeding *et al.* (*6, 7*) reported that methanol can be converted selectively to C_2–C_4 olefins over P-modified ZSM-5 catalysts. They found that catalysts prepared from trimethylphosphite, calcined in air, show an increase in the number of acid sites and a decrease in their acid strength compared to the unmodified ZSM-5. This was concluded on the basis of the results of the ammonia desorption technique of Kerr and Chester (*8*) and a model of permanent attachment of phosphorus through oxygen to the zeolite framework was proposed. These results suggested that incorporation of phosphorus converts the strong acid sites into weaker ones, possibly Lewis acid sites. Different views were held by Haber *et al.* (*9*) who found by TPD of ammonia that the introduction of phosphorus using trimethylphosphite and diammonium hydrogen phosphate eliminates the Brønsted acid sites and also significantly decreases the content in weaker acid sites. Later Vedrine *et al.* (*1*) found that phosphorus neutralizes acidic sites primarily at the entrance of the channels of the zeolite particles. It was also reported that the strongest acidic sites inside the channels remained unmodified by treatment with phosphorus. Nunan *et al.* (*5*) concluded from poisoning experiments with quinoline and trimethylphosphite that the most important effect of phosphorus is the poisoning of the strong acid sites on the exterior of the crystals. Neither interpretation is in agreement with those of Kaeding *et al.* (*6, 7*). There is no general agreement in the literature either on the structure of the supported phosphorus phase or the characteristics of the structure which determine paraselectivity. The preparation of P/ZSM-5 catalysts is described in detail in Refs. (*10, 11*). Diphenylphosphine chloride, trimethylphosphite, phosphorus trichloride, and phosphoric acid are some of the numerous compounds which were used as the source of phosphorus.

To date very little quantitative spectroscopic information on the location and nature of phosphorus species on H–ZSM-5 is available. The objectives of the present work are thus to characterize the structure

[1] To whom correspondence should be addressed.

0021-9517/88 $3.00

of the phosphorus deposited on a ZSM-5 support by the gas-phase adsorption of triphenylphosphine and to relate these observations to the catalytic properties of the so-prepared solids, in the MTG reactions. The methods of characterization encompassed a quantitative treatment of infrared spectra of adsorbed pyridine adapted from that originally proposed by Rhee *et al.* (*23*) and analyses of ESCA data including binding energy shifts at the various stages of the preparation procedure and intensity ratios of the calcined catalysts. In this last case, a very recently proposed method (*16*) for the treatment of ESCA intensity data of calcined samples obtained before and after grinding was utilized in order to calculate the respective contents and average crystallite size of the phosphorus located inside and outside the pore lattice.

EXPERIMENTAL

Catalyst Preparation

ZSM-5 samples were synthesized according to a method described as method B′ by Gabelica *et al.* (*12*). Activation of zeolite samples is performed by repeated ion exchange with NH_4NO_3 solutions followed by calcination in air at 500°C. The ZSM-5 sample was characterized by X-ray diffraction (XRD) on a Phillips spectrometer equipped with PW010 generator and PW1050 goniometer. Spectra were recorded using the Cu$K\alpha$ ray excitation. Scanning electron micrographs (SEM) were taken using a JEOL Model 2553 microscope (*13*). Both results indicate that ZSM-5 samples are made of highly crystalline, 1- to 5-μm spherical agglomerates of microcrystals. Elemental analysis for the measurements of Si/Al ratio (Si/Al = 41) have been done by PIXGE (*14*) and confirmed by atomic absorption.

Triphenylphospine $(C_6H_5)_3P$ was purchased from Strems Chemicals. It was deposited following an original method designated as the gas-phase adsorption (GPA) of an organic complex (*13*). In this technique, the triphenylphosphine was heated with the zeolite in a glass tube preliminary evacuated and sealed. The temperature was then maintained at 400°C for 16 hr and the system was cooled to room temperature and opened under ambient conditions. Analyses were performed before and after air calcination at 400°C.

A first series of catalysts was prepared with the highest target phosphorus content (1.2 wt%) corresponding to the stoichiometric amount necessary for complete poisoning of all Brønsted acid sites. The phosphorus contents actually measured in the calcined catalysts were 0.3, 0.4, 0.7, and 0.8 wt% P in ZSM-5. They were designated as P1/H–ZSM-5, P2/H–ZSM-5, P3/H–ZSM-5, and P4/H–ZSM-5, respectively. Another catalyst designed to present a higher proportion of extraparticle phosphorus was prepared by the same technique, with a total loading of 2.4 wt% P in the calcined state. This catalyst was designated P5/H–ZSM-5. The weight percentage of phosphorus in the final sample was measured by atomic absorption. X-ray diffraction analysis showed no loss of crystallinity both before and after the calcination. No new XRD lines were observed in addition to the pattern of the support.

CATALYST CHARACTERIZATION

IR of Adsorbed Pyridine

Systemic infrared of adsorbed pyridine was performed on all calcined samples in order to determine the level of substitution of protonic acid sites in ZSM-5. Thin self-supporting wafers of roughly 6 mg of the sample were prepared by placing the powdered material in a stainless-steel die having a diameter of 13 mm and compressing under a force greater than 15,000 lb for 1 min. The wafers were mounted on a stainless-steel sample holder and installed into a five-sample quartz-Pyrex vacuum cell. The wafers were then calcined *in situ* at 400°C while evacuating (10^{-6} Torr) for 20 hr. After cooling to room temperature, a spectrum was recorded. Pyridine vapor adsorption was accomplished for 5 min. Afterward, the

cell was degassed and evacuated (10^{-6} Torr) at a temperature of 200°C for 16 hr to eliminate completely the physisorbed pyridine before the recording of another spectrum. All spectra were recorded from 4000 to 1,000 cm^{-1} using a digilab FTS-60 instrument with 2 cm^{-1} resolution.

ESCA

Dispersion and oxidation states of P1, P2, P3, and P4/H–ZSM-5 calcined and uncalcined samples and P5/H–ZSM-5 calcined sample were studied by X-ray photoelectron spectroscopy (ESCA). Spectra were acquired on a VG ESCALAB Mark II electron spectrometer equipped with a hemispherical electron analyzer. Samples were mounted in stainless-steel cups and analyzed in the constant pass energy mode (20 eV), using an incident beam of Mg$K\alpha$ X-rays. Pressure in the chamber during spectral acquisition was less than 10^{-6} Pa. All binding energies were corrected for charging by referencing the binding energy scale to Si_{2P} at 103.4 eV. Calcined catalysts P1, P2, P3, and P4/H–ZM-5 were ground for 30 min in a mortar and XPS spectra were taken under the same conditions as the unground samples.

Catalytic Tests

Methanol-to-gasoline (MTG) reactions were carried out at atmospheric pressure and at 400°C in a microcatalytic fixed-bed reactor, made of 38-cm-long SS tube with a 6-mm i.d. One gram of catalyst was placed between two plugs of glass wool in the middle of the reactor. The catalyst was introduced in the reactor freshly calcined and no further pretreatment was performed. Methanol (99.99% pure from Fisher) was fed 2 hr into the reactor using a HPLC Gilson pump for injection in a helium gas stream. A helium flow rate of 30 ml STP/min and a constant methanol WHSV of 1.4 hr^{-1} were maintained for all runs. Condensed fractions were collected separately at 0 and −80°C and noncondensed products were sampled at selected time intervals with a 16-loop Valco valve controlled by a sequence programmer. All products were analyzed using a Perkin–Elmer Sigma 15 gas chromatograph equipped with two Porapak Q columns. From the analysis of the various products collected, the weight percent of each product in the stream leaving the reactor was calculated. A more detailed description of the setup and analytical procedures is given in (*15*).

RESULTS

FTIR Spectroscopy

Figure 1 shows infrared spectra in the regions 1400–1600 (after pyridine adsorption) and 3000–4000 cm^{-1} (before pyridine adsorption). After adsorption of pyridine, the bands due to chemisorbed pyridine were observed at approximately 1546 and 1457 cm^{-1}, respectively. At the same time, the 3610 cm^{-1} band, assigned to the Al–OH band disappears due to the formation of pyridinium ions. The line assigned to Si–OH vibrations, which appears at 3740 cm^{-1}, is not affected by pyridine adsorption. For P5/H–ZSM-5, which contains the highest amount (2.4%) of phosphorus, both bands at 3610 and 3740 cm^{-1} are attenuated after

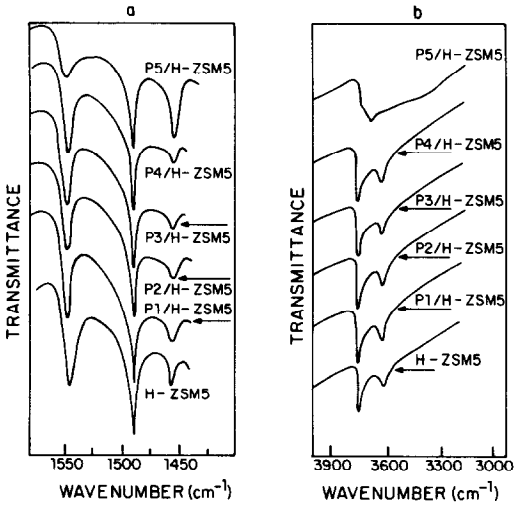

FIG. 1. (a) Infrared spectra in the region 1400–1600 cm^{-1} after pyridine adsorption and (b) IR spectra in the region 3000–4000 cm^{-1} before pyridine adsorption.

phosphorus deposition, and a new band appears at 3685 cm^{-1}.

The bands at 1546 and 1457 cm^{-1} indicate the presence of both Brønsted and Lewis acid sites, respectively. A third band at wavenumber 1491 cm^{-1} is due to contributions of both Lewis and Brønsted acid sites.

An estimation of the ratio of the number of Brønsted acid sites to Lewis acid sites is obtained by

$$\frac{B}{L} = \frac{A_B}{A_L} \times (\varepsilon_L/\varepsilon_B), \qquad (1)$$

where A_B/A_L is the IR absorbance ratio and $\varepsilon_L/\varepsilon_B$ is the extinction coefficient ratio. Rhee *et al.* (*23*) found that $\varepsilon_L/\varepsilon_B$ asymptotically approaches 1.5 for $SiO_2/Al_2O_3 > 15$. The unit cell of the H–ZSM-5 support is expressed as $Al_{2.27}Si_{93.73}O_{192}$ and upon dehydroxylation, two Brønsted sites must be destroyed for each Lewis site created:

$$B_Z = 2.27 - 2L_Z. \qquad (2)$$

Applying Eq. (1) to the support gives an equation between B_Z and L_Z, which can be solved simultaneously with Eq. (2) to yield the values for B_Z and L_Z, $B_Z = 1.8$ and $L_Z = 0.26$ per unit cell.

Assuming that one P is exchanged for one Brønsted site and no Lewis site is created in this exchange, the following equation can be developed:

$$(P) = B_Z - B = B_Z - (2.27 - B_Z)(\varepsilon_L/\varepsilon_B)(A_B/A_L), \qquad (3)$$

where (P) represents the number of phosphorus-containing ions exchanged per unit cell. These results also expressed either as the number of unexchanged Brønsted sites (B) or as the weight percent of exchanged phosphorus (wt% P) are presented in Table 1 for calcined catalysts.

TABLE 1

Quantitative IR Analysis of Adsorbed Pyridine

Sample	$\nu_{Brønsted}$ (cm^{-1})	ν_{Lewis} (cm^{-1})	A_B/A_L[a]	P/u.c.[b]	B/u.c.	Weight percent P exch.
H–ZSM-5	1546	1457	4.6	—	1.8	—
P1/H–ZSM-5	1546	1457	3.64	0.38	1.42	0.20
P2/H–ZSM-5	1548	1456	3.25	0.53	1.27	0.28
P3/H–ZSM-5	1545	1457	3.18	0.56	1.24	0.30
P4/H–ZSM-5	1545	1456	3.16	0.57	1.23	0.31
P5/H–ZSM-5	1546	1445	0.69	1.53	0.27	0.82

[a] Ratio of absorbances at $\nu_{Brønsted}$ (A_B) and ν_{Lewis} (A_L).
[b] Calculated from Eq. (3); u.c., unit cell of the ZSM-5 support $Al_{2.27}Si_{93.73}O_{192}$.

Photoelectron Spectroscopy

The binding energy for O_{1S}, Al_{2p}, P_{2p}, and C_{1s} and ESCA intensities as well as atomic ratios calculated from intensity ratios are presented in Table 2 for both calcined and uncalcined unground samples, and in Table 3 for calcined ground samples. All binding energy values were obtained with a precision of ±0.1 eV, with the exception of C_{1s} for uncalcined samples and O_{1s} and Al_{2p} for calcined samples. These values were obtained from the survey with a precision of ±0.5 eV.

Ratios of atomic concentrations in the first layers of the sample are estimated from the corresponding ESCA peak area ratios using the relationship

$$\left(\frac{P}{Si}\right)_{XPS} = \frac{n_P}{n_{Si}} = \frac{A_P}{A_{Si}} \cdot \frac{\sigma_{Si}}{\sigma_P} \cdot \frac{\lambda_{Si}}{\lambda_P} \cdot \frac{D_{Si}}{D_P}, \qquad (4)$$

where σ is the cross section of the emission of photoelectrons, λ is the escape depth, n_P/n_{Si} is the ratio of atomic densities of phosphorus and silicon, respectively, and D_P/D_S is the electron detection efficiency ratio, which for the VG ESCALAB II equals $(E_{KP}/E_{KS})^{-1/2}$ where E_K stands for the kinetic energy of the emitted electron.

To estimate particle size data from XPS intensity measurements, a model developed by Kaliaguine *et al.* (*16*) was employed. The model is similar to that of Kerkhof and Moulijn (*17*) but it deals simultaneously with the effects of both dispersion and surface segregation in the representation of ESCA intensity ratios. It is assumed that the catalyst consists of stacks of sheets of the support with the supported phase particles in between these sheets.

TABLE 2

ESCA Data for Calcined and Uncalcined Samples

Sample	$(P/Si)_{BULK}$ $\times 10^3$	ΔE^a charge (eV)	O_{1S} (eV)	Al_{2p} (eV)	P_{2p} (eV)	C_{1S} (eV)	I_{Si2p} $\times 10^{-3}$	I_{P2p} $\times 10^{-3}$	I_P/I_{Si} $\times 10^3$	I_C/I_P	$(P/Si)_{ESCA}$ $\times 10^3$	$(C/P)_{ESCA}$
H-ZSM-5	—	5.0	533.0	75.3	—	—	20.33	—	—	—	—	—
P1/H-ZSM-5												
Calcined	6.0	4.6	533.0	75.3	136.1	—	18.509	0.289	15.6	—	10.9	—
Uncalcined		3.5	532.9	75.1	135.6	285.5	16.715	0.315	18.8	6.13	13.1	7.91
P2/H-ZSM-5												
Calcined	8.2	4.4	533.2	75.2	136.1	—	23.125	0.638	27.6	—	19.2	—
Uncalcined		3.3	533.2	75.3	135.3	285.8	15.403	0.587	38.1	8.54	26.5	11.02
P3/H-ZSM-5												
Calcined	13.9	4.5	533.2	75.6	136.2	—	21.17	0.791	37.4	—	25.9	—
Uncalcined		2.4	533.5	75.3	134.9	286.6	11.63	0.815	70.1	9.88	48.7	12.74
P4/H-ZSM-5												
Calcined	16.0	4.8	533.1	75.5	136.1	—	15.216	0.563	37.0	—	25.7	—
Uncalcined		2.3	532.7	75.0	133.4	286.7	11.02	0.795	72.0	10.86	50.2	14.00
P5/H-ZSM-5												
Calcined	48.0	4.7	533.8	75.0	134.9	—	14.08	0.733	52.06	—	36.2	—

[a] Calculated by taking Si_{2p} at 103.4 eV.

For unground catalyst the uneven repartition of supported species was represented by a population of small crystals, with size C_1, being homogeneously dispersed over the entire surface of the catalyst, while another population of larger crystals of size C_2 are segregated on the external surface of the support. For the ground catalysts, it was assumed that the two populations are homogeneously dispersed over the entire surface of the catalyst. The total loading $x_B = x_1 + x_2$, where x_1 and x_2 are the respective weight percents of crystallites with sizes C_1 and C_2. Table 4 represents the results for C_2 and x_1, calculated by solving simultaneously the two equations given in Ref. (*16*) for ground and unground catalysts and using the two series of experimental values for $(I_{P_{2p}}/I_{Si_{2p}})_{ESCA}$.

In the calculations, the following values have been used: density of SiO_2, $\rho_S = 2.4$ g/cm^3, and P_2O_5, $\rho_p = 2.39$ g/cm^3; N_2 BET surface area of the support $S_0 = 350$ m^2/g; external surface area $A_0 = 10$ m^2/g, a value adopted for ZSM-5 with similar crystal size and habit (*18*); escape depth for Si_{2p}, $\lambda_{Si} = 24$ Å, and P_{2p}, $\lambda_p = 20$ Å (*19–21*); cross section of the emission for Si_{2p}, $\sigma_{Si} = 0.865$, and for P_{2p}, $\sigma_p = 1.25$ (*22*); calculated ratio of atomic densities of supported phase and support $n_P/n_S = 0.946$; $E_{KP} = 1108.7$ eV; and $E_{KS} = 1141.4$ eV. The value of C_1 was arbitrarily chosen as 3 Å, considering the pore size and geometry of the zeolite ZSM-

TABLE 3

ESCA Data for Ground Catalysts

Sample	$(P/Si)_{BULK}$ $\times 10^3$	ΔE^a charge (eV)	O_{1S} (eV)	Al_{2p} (eV)	P_{2p} (eV)	I_{Si2p} $\times 10^{-3}$	I_{P2p} $\times 10^{-3}$	I_P/I_{Si} $\times 10^3$	$(P/Si)_{ESCA}$ $\times 10^3$
P1/H-ZSM-5	6.0	5.2	533.8	75.4	135.8	13.65	0.230	15.00	11.71
P2/H-ZSM-5	8.2	5.2	533.8	75.6	135.6	16.42	0.413	25.15	17.48
P3/H-ZSM-5	13.9	4.9	534.0	75.5	135.5	18.52	0.556	30.02	20.86
P4/H-ZSM-5	16.0	4.9	534.0	75.6	135.7	14.53	0.428	29.46	20.48

[a] Calculated by taking Si_{2p} at 103.4 eV.

TABLE 4

Values of Weight Percent Dispersed Fraction (x_1) and Segregated Crystal Size (C_2) Calculated from the ESCA Model in (*16*)

Sample	x_B (wt%)	$(I_P/I_{Si})_{XPS}$ ratio		Calculated from two XPS intensity ratio	
		Unground catalyst	Ground catalyst	x_1%	C_2 (Å)
P1/H–ZSM-5	0.3	0.0156	0.0150	0.20	233
P2/H–ZSM-5	0.4	0.0276	0.0252	0.29	267
P3/H–ZSM-5	0.7	0.0374	0.0300	0.34	307
P4/H–ZSM-5	0.8	0.0370	0.0295	0.33	397

5. It was found by Kaliaguine *et al.* (*18*) that if C_1 varies from 3 to 10 Å, C_2 is not changed by more than a few percent.

Catalytic Tests

Results of the standard MTG test performed on H–ZSM-5 and all phosphorus/H–ZSM-5 samples are presented in Table 5. Methanol conversion to hydrocarbons and water is complete in all cases. From the percentage of H_2, CO, and CO_2 determined in the products one can calculate a percentage of methanol decomposed to CO and H_2 (designated as $(H_2 + CO)_{calc}$), and a weight percent of water transformed by water gas shift (H_2O_{WGS}). Both quantities are essentially not affected by the presence of phosphorus. According to the general reaction pathway of MTG reaction (*24*),

$$2CH_3OH \rightleftharpoons CH_3OCH_3 \rightarrow C_2\text{–}C_5 \text{ Olefins} \rightarrow \begin{matrix}\text{Paraffins}\\ \text{Aromatics}\\ \text{Cycloparaffins}\\ C_5^+ \text{ olefins}\end{matrix}$$

TABLE 5

Results of MTG Tests

Catalyst:	H–ZSM-5	P1/H–ZSM-5	P2/H–ZSM-5	P3/H–ZSM-5	P4/H–ZSM-5	P5/H–ZSM-5
Conversion (%):	100	100	100	100	100	100
Product distribution (wt%)						
$(CO + H_2)_{calc}$	0.6	1.0	0.2	0.5	0.7	0.7
H_2O_{expt}[a] + H_2O_{WGS}[b]	55.1	52.8	56.1	55.4	55.9	52.9
% WGS[c]	0.1	0.05	0.06	0.06	0.03	0.06
Hydrocarbons	44.3	46.2	43.7	44.1	43.4	46.4
Hydrocarbon distribution (wt%)						
CH_4	0.8	0.8	0.6	0.6	0.5	0.7
C_2–C_4 paraffins	51.4	57.0	44.2	44.1	40.3	14.0
C_2–C_4 olefins	2.7	5.8	8.2	11.0	9.1	45.1
% olefins in C_2–C_4	4.9	9.2	15.6	19.9	18.5	76.3
C_5^+	45.1	36.4	46.9	44.3	50.1	40.1
Aromatics A_6–A_{10}	30.3	23.4	27.8	24.7	29.3	11.2
% aromatics in C_5^+	66.5	64.3	59.3	55.9	59.7	28.0
% H in hydrocarbons	51.6	51.1	50.5	51.9	50.9	52.9
Production of aromatics (g/2 hr)	0.37	0.31	0.34	0.35	0.36	0.14

Note. Operating conditions: temperature 400°C, pressure 1 atm, WHSV 1.4 hr^{-1}, helium flow rate 30 ml STP/min.

[a] Amount of water measured in the reaction products.

[b] Amount of water converted by WGS (calculated from CO_2 production).

[c] % WGS = $100 \times H_2O_{WGS}/[H_2O_{expt} + H_2O_{WGS}]$.

the changes in activity are best illustrated by the change in olefin content in the C_2–C_4 fraction and aromatics in C_5^+ fraction of the products, since methanol and dimethyl ether conversions are 100% in all cases. An increase in the relative yield of C_2–C_4 olefins upon phosphorus deposition and a decrease in aromatic production are observed for all catalysts. Figure 6 represents the proportion of propylene in C_3 products as a function of the number of Brønsted acid sites present in the sample determined from IR of adsorbed pyridine. It is observed in Fig. 6 that by selective poisoning of ZSM-5 with phosphorus, it is possible to increase dramatically the yields in light olefins.

Figure 7 represents the proportion of the different hydrocarbon chain lengths obtained in the products of a MTG test. For P5/H–ZSM-5 higher amounts of olefins and lower amounts of aromatics were obtained compared to other samples and cyclohexene was the main C_6 product.

DISCUSSION

Figure 1a shows the spectra of pyridine adsorbed on the various catalysts. A continuous decrease in the absorbance ratio of the 1545 to 1456 cm^{-1} lines (A_B/A_L) is observed as the phosphorus content is increased. This variation is indicative of the progressive poisoning of the Brønsted acid sites by phosphorus species. Figure 1b shows the OH vibration bands of the calcined catalysts before pyridine adsorption. The P1 to P4/ZSM-5 catalysts show the same two lines as the support, namely the 3740 cm^{-1} band corresponding to silanol Si–OH groups and the 3610 cm^{-1} band usually associated with the acidic Al–OH groups. Upon pyridine adsorption the 3740 cm^{-1} is almost not affected whereas the 3610 cm^{-1} band disappears completely. These spectra suggest therefore that at low-P content these catalysts (up to 0.8%) contain no new OH group. Only in the P5/ZSM-5 catalysts, containing 2.4% P, is a new line observed at 3685 cm^{-1}. This suggests that the new OH group is associated with the phosphorus oxidic phase located on the external surface of the support, which is only abundant in the P5/ZSM-5 sample. Upon pyridine adsorption the 3685 cm^{-1} line is only slightly affected which suggests that the corresponding OH group is not acidic.

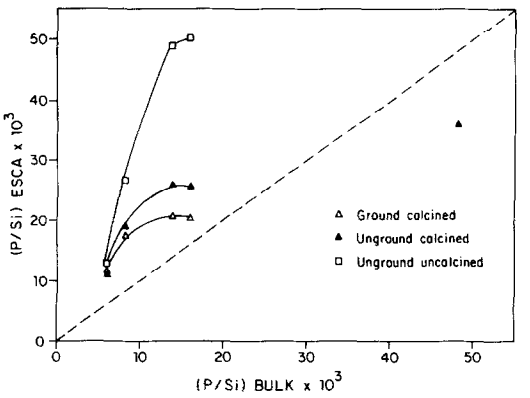

FIG. 2. $(P/Si)_{ESCA}$ atomic ratio calculated from ESCA intensity ratio as a function of bulk atomic ratio $(P/Si)_{bulk}$.

Figure 2 gives the values of atomic ratio P/Si calculated from ESCA intensity ratio $I_{P_{2p}}/I_{Si_{2p}}$ using Eq. (4), as a function of the bulk value for P/Si. The upper curve corresponds to the samples after triphenylphosphine adsorption, before calcination. As this curve lies well above the $y = x$ line, it must be concluded that phosphorus is both surface segregated and well dispersed in these samples. Calcination results in a significant decrease in $(P/Si)_{ESCA}$ which could correspond either to a penetration of the phosphorus species in the pore lattice or/and to a sintering or agglomeration of the phosphorus-containing phase upon calcination. As the ground samples yield lower values of the $(P/Si)_{ESCA}$ ratio than the unground ones, it must be concluded that phosphorus is at least partially surface segregated in the calcined catalysts P1 to P4/ZSM-5.

In Fig. 3, values for the $(C/P)_{ESCA}$ calculated from intensity ratios for C_{1S} and P_{2p} ESCA lines using the adapted version of Eq. (4) are reported as a function of the

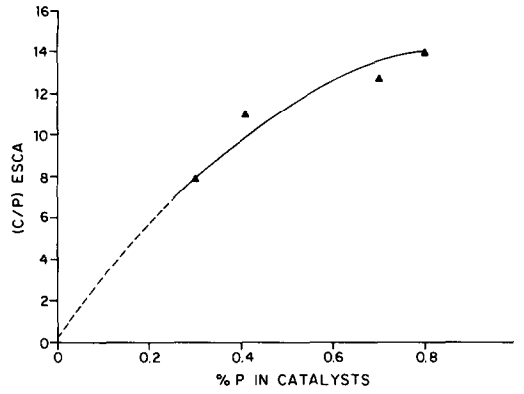

FIG. 3. Atomic ratio of $(C/P)_{ESCA}$ calculated from ESCA intensity ratio as a function of bulk weight percent phosphorus.

bulk weight percent of phosphorus in noncalcined samples P1 to P4/ZSM-5. If the triphenylphosphine had no chemical interaction with the support, a value of 18 would be expected for C/P. As the values for sample P2–P4/ZSM-5 are closed to 12 (see Table 2) it may be suggested that P species bearing two aromatic rings are predominantly adsorbed on these catalysts. The value close to eight for the $(C/P)_{ESCA}$ ratio in sample P1/ZSM-5 suggests that at low-P loading a higher proportion of more converted phosphine species, bearing for example only one phenyl, is present. These suggestions are supported by the values of the P_{2p} binding energies reported in Table 2 for noncalcined catalysts, which shows a progressive decrease from 135.6 eV in P1/ZSM-5 go 133.4 eV in P4/ZSM-5. As the reported value (*25*) for P_{2p} in triphenylphosphine is 130.6, it is believed that the progressive addition of phenyl ligands to trivalent phosphorus would be responsible for the observed shift. Interestingly as shown in Fig. 4 this progressive shift of the P_{2p} binding energy is accompanied by a shift in the opposite direction of the C_{1S} level, indicating electron transfer from the aromatic ring to the phosphorus atom. In Fig. 4, the C/P value for triphenylphosphine was arbitrarily chosen as 18.

From the I_P/I_{Si} values for the calcined catalysts P1–P4/ZSM-5 reported in Tables 2 and 3 for unground and ground samples, the values for x_1 and C_2 were calculated using the equations developed in Ref. (*16*) x_1 is the weight percent of the phosphorus fraction located within the pores, whereas x_B is the bulk weight percent of phosphorus, so that the loading of segregated phosphorus in these catalysts stays between 0.10 and 0.47%. The average size C_2 of the crystallites of this segregated phase varies from 233 to 397 Å.

In Fig. 5 the values for the weight percent

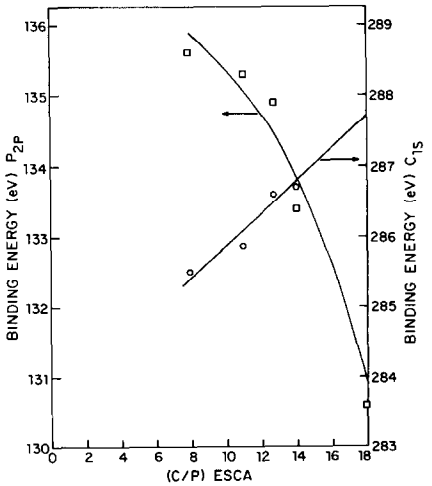

FIG. 4. Binding energy (eV) shift of P_{2p} and C_{1S} as a function of $(C/P)_{ESCA}$.

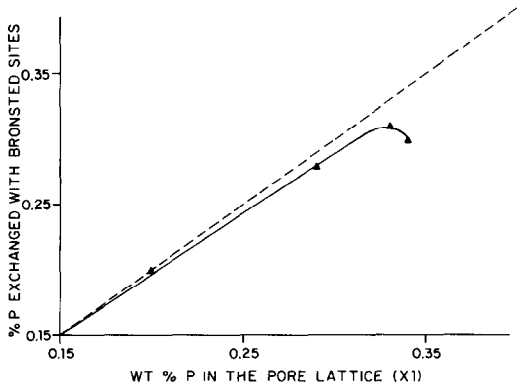

FIG. 5. Weight percent phosphorus exchanged with Brønsted acid sites as a function of weight percent dispersed fraction (x_1) calculated from ESCA data.

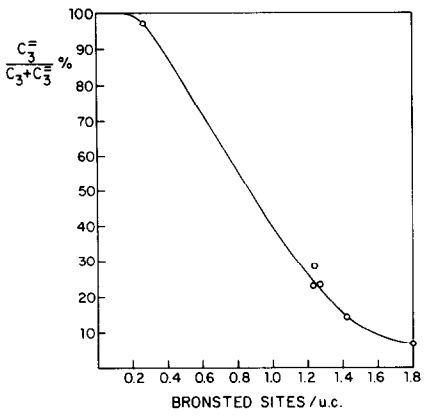

FIG. 6. MTG tests—weight percent propylene in C_3 fraction as a function of Brønsted acid sites per unit cell.

of phosphorus exchanged with Brønsted acid sites in calcined catalysts, determined by IR of adsorbed pyridine and reported in Table 1, are plotted as a function of x_1, the weight percent of the well-dispersed phosphorus located within the pores, calculated from ESCA intensity ratios and reported in Table 4. The agreement between the two sets of values is surprisingly good, suggesting that in these four samples almost every phosphorus atom having penetrated the pores has substituted a Brønsted acid site. It seems thus that the phosphorus species derived from triphenylphosphine are extremely active poisons of these sites. One possible mechanism for this poisoning is shown in Fig. 8.

In Fig. 8, a model is also proposed for the pentavalent phosphorus species obtained upon calcination of diphenyl intermediates. This structure may be considered the dehydrated version of that proposed by Kaeding and Butter (*7, 27*). The dehydroxylated form is preferred here because as discussed above no new OH band appears in the IR spectra of calcined samples P1, P2, P3, and P4/ZSM-5 compared to the spectrum of the support.

From Table 5 it is apparent that the fraction of olefins in C_2–C_4 hydrocarbons and the production rate of aromatics are strongly dependent on the bulk phosphorus content. In Fig. 6 it is shown for example that the proportion of propylene in C_3 is well correlated with the concentration of nonpoisoned Brønsted acid sites, determined from IR of adsorbed pyridine. Obviously very high olefin contents and very low conversion to aromatics may be expected under standard conditions for Brøn-

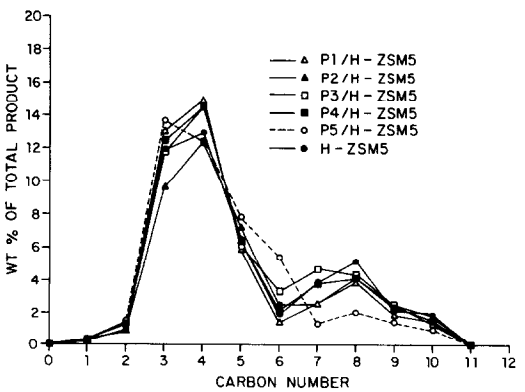

FIG. 7. Distribution of carbon numbers in the hydrocarbon products of MTG tests.

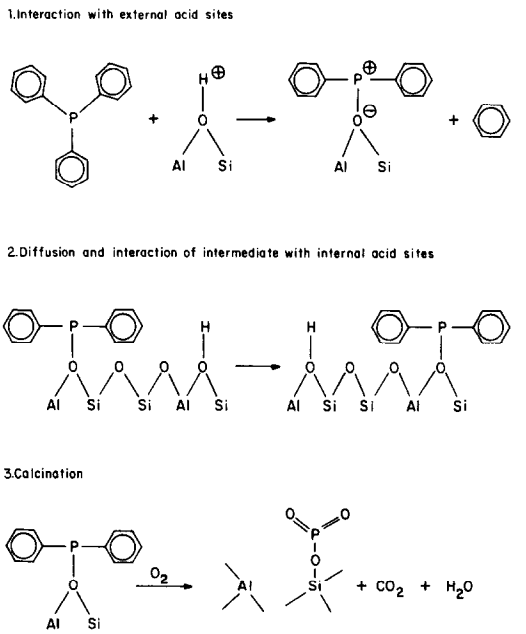

FIG. 8. Mechanism for phosphorus binding to the zeolite framework.

sted sites concentrations below 0.3 per unit cell. The ESCA study did show that using the GPA technique such levels of exchange are only reached for high-P loadings when a large proportion of the phosphorus is surface segregated. Figure 7 shows the carbon number distribution in the products of the standard MTG test. Only with the P5/ZSM-5 sample is the fraction of C_6^+ noticeably decreased. It is interesting to note that the C_6 hydrocarbons obtained with this catalyst are essentially containing cyclohexene. This confirms that cycloolefins are intermediate in the production of aromatics from olefins (*26*).

CONCLUSION

This work illustrates the importance of the ESCA technique in the study of modified zeolites. The data for C/P ratios calculated from ESCA intensity ratios suggest that in the noncalcined catalysts, phosphorus is mainly present as in diphenyl intermediates. At very low loadings (0.3%) more converted P species are present on the surface suggesting that triphenylphosphine interacts first with pairs of Brønsted acid sites. These pairs being very low in concentration are rapidly saturated and the diphenyl species dominates when P loading is increased.

The results of Fig. 2 which show a clear decrease in $(P/Si)_{ESCA}$ ratio can be interpreted by a diffusion of the diphenyl intermediates into the pore lattice during calcination. According to this model all phosphorus atoms located inside the pore channels would be in ionic species exchanged for Brønsted acid sites. Such a situation is strongly supported by the results shown in Fig. 5 which indicate that the IPL phosphorus loading calculated from ESCA data (x_1) is identical, in low phosphorus samples, with the phosphorus loading in cationic species having substituted Brønsted sites, and determined independently from IR of adsorbed pyridine data. This exchange is therefore viewed as the poisoning mechanism which leads to increased olefin contents and decreased aromatic production rates during MTG reactions.

REFERENCES

1. Védrine, J. C., Auroux, A., Dejaifve, P., Ducarne, V., Hoser, H., and Zhou, S., *J. Catal.* **73,** 147 (1982).
2. Lercher, J. A., and Rumplmayr, Q., *Appl. Catal.* **25,** 215 (1986).
3. Cai, G. Y., Chen, G. Q., Qang, Q. X., Xin, Q., Wang, X. A., Wang, Z. Z., Li, X. Y., and Liang, J., *Stud. Surf. Sci. Catal.* **24,** 319 (1985).
4. Balkrishnan, I., Rao, B. S., Hegde, S. G., Kotasthane, A. N., Kulkarni, S. B., and Ratnaswamy, P., *J. Mol. Catal.* **17,** 261 (1982).
5. Nunan, J., Cronin, J., and Cunningham, J., *J. Catal.* **87,** 77 (1984).
6. Young, L. B., Butter, S. A., and Kaeding, W. W., *J. Catal.* **76,** 418 (1982).
7. Kaeding, W. W., and Butter, S. A., *J. Catal.* **61,** 155 (1980).
8. Kerr, G. T., and Chester, A. W., *Therm. Chim. Acta* **3,** 113 (1971).
9. Derewinski, M., Haber, J., Ptaszynski, J., Shiralkar, V. P., and Dzwigaj, S., *Stud. Surf. Sci. Catal.* **18,** 209 (1984).
10. U.S. Patent 4,000,698 (1977). [Mobil]
11. U.S. Patent 3,972,832 (1976). [Mobil]
12. Gabelica, Z., Derouane, E. G., and Blom, N., *Appl. Catal.* **5,** 227 (1983).
13. Mahay, A., Lemay, G., Adnot, A., Szoghy, I. M., and Kaliaguine, S., *J. Catal.* **103,** 480 (1987).
14. Szoghy, I., Mahay, A., and Kaliaguine, S., *Zeolites* **6,** 39 (1986).
15. Mahay, A., Ph.D. thesis, Université Laval, 1986.
16. Kaliaguine, S., Adnot, A., Lemay, G., and Rodrigo, L., *J. Phys. Chem.*, submitted for publication.
17. Kerkhof, F. P. J. M., and Moulijn, J. A., *J. Phys. Chem.* **83,** 1612 (1979).
18. Kaliaguine, S., Adnot, A., and Lemay, G., *J. Phys. Chem.* **91,** 2886 (1987).
19. Vulli, M., and Stark, K., *J. Phys. E* **10,** 158 (1977).
20. Chang, C. C., *Surf. Sci.* **48,** 9 (1975).
21. Penn, D. R., *J. Electron Spectrosc. Relat. Phenom.* **9,** 29 (1976).
22. Scofield, J. H., *J. Electron Spectrosc. Relat. Phenom.* **8,** 129 (1976).
23. Rhee, K. H., Rao, U. S., Stencel, M., Melson, G. A., and Crawford, J. E., *Zeolites* **3,** 337 (1983).

24. Chang, C. D., and Silvestri, A. J., *J. Catal.* **47,** 249 (1977).
25. Pelavin, M., Hendrickson, D. N., Hollander, J. M., and Jolly, W. L., *J. Phys. Chem.* **74,** 1116 (1970).
26. Van Hooff, J. H. C., *in* "Chemistry and Chemical Engineering of Catalytic Processes" (R. Prince and G.C.A. Schuit, Eds.), NATO *Adv. Stu. Ins.* Series, Vol. 39, p. 599. 1980.
27. Kaliaguine, S., B. Nagy, J., and Gabelica, Z., *in* "Keynotes in Energy-Related Catalysis" (S. Kaliaguine, Ed.), Studies in Surface Science and Catalysis, No. 35, p. 392. Elsevier, Amsterdam, 1988.